energies

MDPI

Article

Stability Improvement of DFIG-Based Wind Farm Integrated Power System Using ANFIS Controlled STATCOM

Varun Kumar *, Ajay Shekhar Pandey and Sunil Kumar Sinha

Electrical Engineering Department, KNIT, Sultanpur 228118, India; ajayshekharpandey@gmail.com (A.S.P.); sinhask98@gmail.com (S.K.S.)

* Correspondence: varun@knit.ac.in

Received: 21 July 2020; Accepted: 6 September 2020; Published: 10 September 2020

Abstract: The stability of the control grid is a critical prerequisite for a safe and efficient power system service. A thorough knowledge of the effects of the power system volatility is essential for the effective study and control of power systems. This paper presents the simulation outcome of a multimachine power network implemented by a wind farm (WF) utilizing a static synchronous compensator (STATCOM) for better stability control objectives. A similarly aggregated double-fed induction generator (DFIG) powered by a gearbox analogy with an equally aggregated wind turbine (WT) determines the operating output of the wind farm. A proportional–integral–derivative controller (PID)-based damping controller, PID including Fuzzy Logic Controller (FLC), and an adaptive network-based fuzzy inference system (ANFIS) controller of the proposed SATCOM are intended to add sufficient damping properties to the dominating modes of the examined system during diverse working circumstances. To assess the feasibility of the suggested control schemes, a frequency-domain method concentrated on a linearized mathematical structure layout utilizing a time-domain strategy centered on a nonlinear configuration of the device that is subjected to severe fault on the attached bus was carried out consistently. A STATCOM damping controller is configured using the ANFIS method to apply appropriate damping properties to the device's decisive modes being evaluated under various test conditions. From the findings of the comparative simulation, it can be inferred that the suggested STATCOM along with the planned ANFIS is seen as comparable to STATCOM with PID and STATCOM with PID plus FLC to increase the stability of the studied device.

Keywords: DFIG-based wind farm; three-machine nine-bus system; STATCOM; stability; fuzzy logic controller; adaptive network-based fuzzy inference system (ANFIS)

1. Introduction

A double-fed induction generator (DFIG) is, due to its numerous strengths, the most functional type of wind turbine. One of its benefits is better performance relative to a fixed speed wind energy network with maximum-scale converters because only around 20% of energy passes across the energy converter and the remainder passes via a stator without electronic regulation. A further benefit of a DFIG-integrated wind farm (WF) is the potential to decouple active power management and reactive capacity to boost grid integration.

The wind farm consisting of a DFIG is linked to the electric network via a line-switched high-voltage direct-current (HVDC), and a damping controller positioned on the HVDC link rectifier current regulator has been suggested to add sufficient dampening to the wind farm under different wind and specific disruption environments. However, such a controlling method proved particularly beneficial to onshore grids with a longer distance to grid systems from the WF [1]. The paper [2]

research displays the concern of power quality attributable to wind turbine integration with the grid. Under this suggested model, to reduce the power quality problems, static synchronous compensator (STATCOM) is attached to a Battery Energy Storage System (BESS) at a point of common coupling (PCC). The usefulness of the implemented system relieves the primary input source from the load and induction generator reactive power demand. At PCC, a STATCOM was linked in ref. [3] to preserve voltage and boost the power output by preventing a DFIG-fed wind energy system linked to a weaker grid by disconnecting throughout and after disruptions. Fuzzy Logic Controller (FLC)-based STATCOM was also used to improve the control reliability of an integrated four-generator two-area power network [4]. Simulation and experimental findings revealed that the hybrid system suggested superior efficiency over a traditional fixed-gain proportional–integral (PI) device. It has been suggested that the scaling factors of a fuzzy with PID-type controller be coordinated with other fuzzy configurations used for the excitation management of a synchronous generator linked to an infinite bus via a transmission line [5]. A STATCOM has produced a greater addition to the transient parameter and Low Voltage Ride Through (LVRT) capacity of fixed speed-based generator-integrated wind farms through measurements and simulations compared to a Static VAR Compensator (SVC)'s output [6]. Nevertheless, the main downside to using a STATCOM was greater harmonics incorporated throughout processes, higher costs, as well as operational costs.

A correlation of dynamic outputs is provided for FACTS tools such as STATCOM and SVC [7]. These tools are used to restore WF together with a multimachine system. The findings obtained show the impact on damping machine fluctuations of SVC and STATCOM-dependent FLC and the increase of device dynamic performance in the post-fault period. This analysis indicates improved dynamic efficiency and a quick failure restoration of STATCOM-based FLC compared to SVC-based FLC across specific fault conditions. A superconducting magnetic energy storage (SMES) focused on adaptive neural artificial network (ANN) has been implemented to boost the dynamic stability of wind farms linked to a multimachine power grid by system fluctuation [8]. Simulation tests conducted using the PSCAD/EMTDC laboratory standard dynamic interface simulator validate the feasibility of the approach proposed. In particular, the proposed SMES improves the intermittent stability of wind farms linked to multimachine system. The adaptive neurocontrol method and analysis, the nonlinear optimal regulation on the multimachine power network, was investigate in ref. [9]. The damping outputs with and without the traditional power system stabilizer (PSS) are also provided for reference. Simulation tests validate that the neurocontroller being studied can achieve better efficiency with respect to transient stability and reliability during various failure situations. The transient enhancement of the stability of a grid-integrated wind farm utilizing a DFIG-dependent flywheel energy storage device was investigated in ref. [10]. To increase the grid-integrated wind farm's transient stability, a cascaded adaptive network-based fuzzy inference system (ANFIS) controller is implemented to an insulated gate bipolar transistor frequency converter. The transient efficiency of the device is analyzed by contrasting the effects of the network utilizing the suggested ANFIS with those of the proportional–integral controllers based on the black-box optimization technique. The system's validity is checked by the results of simulation conducted using the PSCAD/EMTDC environment. A contrast of the output of the ANN-SSSC (Static Synchronous Series Compensator)-based combined wind farm (CWF), CWF fed by ordinary SSSC, and CWF with Multiobjective Genetic Algorithm based (MOGA)-based SSSC is rendered to see the motivation of ref. [11]. The findings are calculated using the root mean square error (RMSE). The findings indicate that CWF's efficiency can be increased by using an ANN-adjusted SSSC. In ref. [12], the effect of the tuned STATCOM on the WF efficiency at strong wind speed and on a WF with an adjusted ANN STATCOM is contrasted with its output when the STATCOM is balanced by the whale optimization algorithm (WOA) and the Multiobjective Genetic Algorithm (MOGA). The findings indicate that with STATCOM tuned by ANN and CWF efficiency can be improved more than with MOGA and WOA. Nevertheless, the disadvantages of the fuzzy inference method were focused solely on the designer's expertise and experience. As FLC and artificial ANN have particular strength, adding both together would give all advantages to a powerful

computational system. The underlying adaptive neuro-fuzzy inference system design and learning process are introduced in ref. [13]. The writers of those articles found an endless bus to be a control system. However, certain synchronous generators (SGs) may be used in an individual large power grid whose reliability may be compromised by modern renewable energy technologies such as an offshore WF.

The approach studied in this research uses a wind farm of large capacity attached to the PCC to design the stabilization properties of an existing power system to evaluate the real power system's operational performance. Throughout this article, the control design is suggested to develop a damping controller such as PID, PID plus fuzzy, and an ANFIS controller to suppress SG system oscillations throughout the order to retain a stable system. The key benefit of this research is the ANFIS-regulated STATCOM, which is regarded as a novel damping controller configured to dampen the studied system's oscillations.

This paper is structured as follows. The device setup and statistical modeling of the studied system including the incorporated WF with STATCOM are presented in Section 2. Section 2.10 describes the model concept and model results for the implemented STATCOM with a PID damping controller utilizing the pole-placement approach. Throughout Section 2.11, the modeled Fuzzy Logic Controller with the PID are defined. The design approach used for the suggested STATCOM ANFIS controller in Section 2.12. Section 3 presents comparable transient outcomes of the analyzed system without a controller as well as with PID, PID with an FLC, and an ANFIS controller exposed to extreme disruption. Section 4 provide a discussion of results. Finally, Section 5 draws clear, significant conclusions from this article.

2. Materials and Methods

2.1. Configuration and Modelling of Test System

Figure 1 shows the observed system setup consisting of a 100.5 MW (67 × 1.5 MW) DFIG-dependent wind farm (WF) as well as a 50 MVAR STATCOM integrated to bus 5 of a nine-bus three-machine network. That WF is described by an aggregated similar DFIG powered from a similar aggregated wind turbine with varying speed via a similar gearbox. The following subsections represents the used mathematical modeling for the test system.

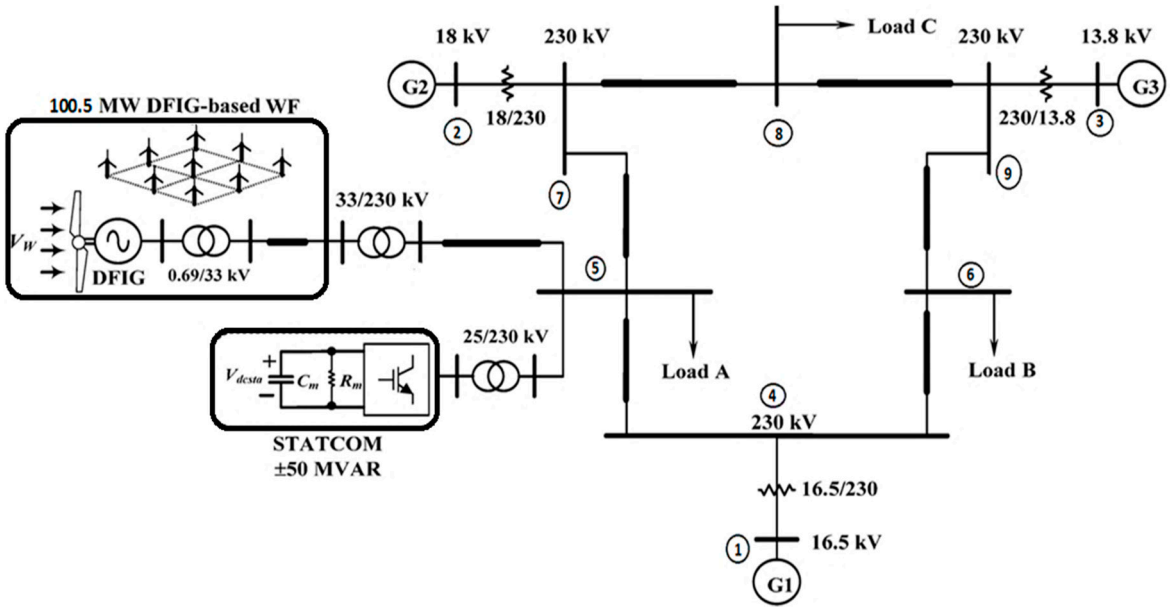

Figure 1. Observe system setup.

2.2. Mathematical Modeling of DFIG-Based Wind Farm

A wound rotor induction generator that is connected to a wind turbine by a gearbox in Figure 2 is used in the DFIG wind turbine. This generator features the direct grid coupled stator and a two-way power converter powering the rotor, which consists of two IGBT bridge–voltage source converters connected to a DC link. This power converter dynamically adjusts the frequency of the grid as well as the frequency of the rotor, permitting varying turbine speeds. The turbine rotor has a blade angle regulation that restricts the strength and rotational speed of heavy winds [14].

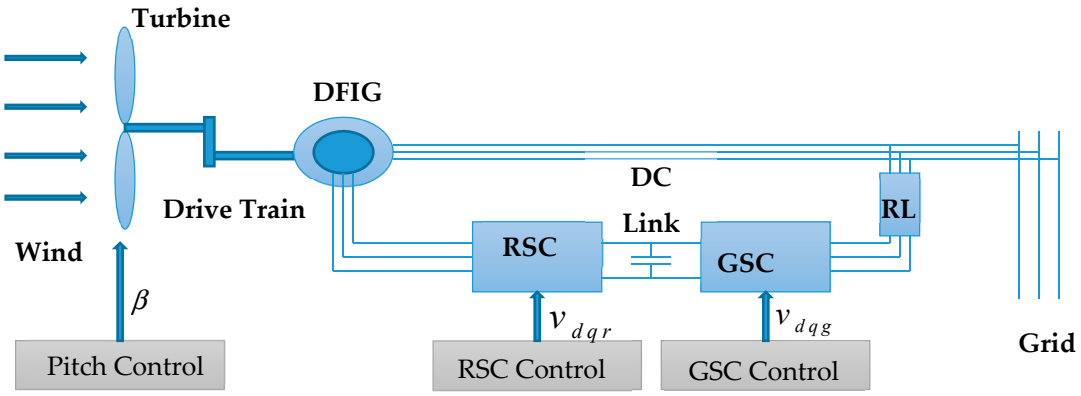

Figure 2. Double-fed induction generator (DFIG) wind turbine.

2.3. Wind Turbine and DFIG Modeling

Wind turbine (WT) mechanical power generation is given as:

$$P_m = \frac{1}{2}\rho A c_p(\lambda,\beta){v_{wind}}^3. \quad (1)$$

c_p is the performance coefficient, which is defined as:

$$c_p = \frac{P_m}{P_{wind}}. \quad (2)$$

The Tip Speed Ratio (TSR) is

$$\lambda = \frac{\omega_r}{v_{wind}}. \quad (3)$$

The performance coefficient is expressed as

$$c_p(\lambda,\beta) = c_1\left(\frac{c_2}{\lambda_x} - c_3\beta - c_4\right)e^{-\left(\frac{c_5}{\lambda_i}\right)} + c_6\lambda \quad (4)$$

$$\frac{1}{\lambda_x} = \frac{1}{\lambda + 0.08\beta} - \frac{0.035}{\beta^3 + 1} \quad (5)$$

where ρ = density of air, A = impact area of blade, v_{wind} = expected wind speed, ω_r = synchronous speed, and β = blade pitch angle.

The drop-in, estimated, and pull-out wind speeds of the WT are 4, 14, and 24 m/s respectively. The wind turbine two-inertia decreased-order comparable mass-spring damper configuration combined with the wind DFIG's rotor shaft is used with an identical gearbox. The equations of motion per unit (pu) can be applied to ref. [14].

The windings designed for the DFIG stator are conveniently attached to a 0.69/33 kV step-up transformer's low-voltage section, whereas the windings on the rotor side DFIG are linked to the same side by a Rotor Side Converter (RSC), DC link, and Grid Side Converter (GSC). The DFIG circuit

diagram is the same as that of the system of induction generator [15]. The DFIG model can be done as follows:

$$\frac{X'_s di_{ds}}{\omega_s dr} = v_{ds} - \left[R_s + \frac{1}{\omega_s T'_o}(X_s - X'_s)\right] \times i_{ds} - (1 - s_r)E'_d - \frac{L_m}{L_{rr}} v_{dr} + \frac{1}{\omega_s T'_o} E'_q + X'_s i_{qs} \quad (6)$$

$$\frac{X'_s di_{qs}}{\omega_s dt} = v_{qs} - \left[R_s + \frac{1}{\omega_s T'_o}(X_s - X'_s)\right] \times i_{qs} - (1 - s_r)E'_q - \frac{L_m}{L_{rr}} v_{qr} - \frac{1}{\omega_s T'_o} E'_d - X'_s i_{ds} \quad (7)$$

$$\frac{dE'_d}{dt} = -s_r \omega_s E'_d + \omega_s \frac{L_m}{L_{rr}} v_{dr} - \frac{1}{T'_o} \times \left[E'_d + (X_s - X'_s) i_{qs}\right] \quad (8)$$

$$\frac{dE'_q}{dt} = -s_r \omega_s E'_d + \omega_s \frac{L_m}{L_{rr}} v_{dr} - \frac{1}{T'_o} \times \left[E'_q - (X_s - X'_s) i_{ds}\right]. \quad (9)$$

The DC link equation can be given as follows

$$C v_{DC} \frac{dv_{DC}}{dt} = v_{dg} i_{dg} + v_{qg} i_{qg} - \left(v_{dr} i_{dr} + v_{qr} i_{qr}\right) \quad (10)$$

where L_{ss} and L_{rr} are the self-inductance of the stator and rotor side respectively; L_m is the mutual inductance; R_s is the resistance of the rotor side; T'_o is the time constant of the rotor circuit; ω_s is the synchronous angle speed; s_r is the rotor slip; X_s is the stator reactance; X'_s is the transient reactance of the stator side; E'_d and E'_q are the voltage behind the transient reactance d-axis and q-axis respectively; i_{ds} represents the d-axis stator currents; i_{qs} represents the q-axis stator currents; V_{ds} and V_{qs} represent the stator voltages of the d and q side, respectively; V_{dr} and V_{qr} are the rotor voltages of the d and q side, respectively. V_{DC} is the DC link voltage; i_{dr} and i_{qr} are the rotor side d and q-axis currents, respectively; i_{dg} and i_{qg} are the grid side d and q-axis currents; V_{dg} and V_{qg} are the grid side d and q-axis voltages, respectively; and i_{DC} is the condenser current.

The rotor section of the converter regulates the power output and monitors the adjustment of the terminal voltage. The diagrams for the control block are seen in Figure 3a. The equations for control are given by [15]:

$$\frac{dx_2}{dt} = i_{qr\_ref} - i_{qr} = K_{p1}\left(P_{ref} + P_s\right) + K_{i1} x_1 - i_{qr} \text{ and } \frac{dx_3}{dt} = v_{s_{ref}} - v_s \quad (11)$$

$$i_{dr\_ref} = K_{p3}\left(v_{s_{ref}} - v_s\right) + K_{i3} x_3 \quad (12)$$

$$\frac{dx_4}{dt} = i_{dr\_ref} - i_{dr} = K_{p3}\left(v_{s_{ref}} - v_s\right) + K_{i3} x_3 - i_{dr} \quad (13)$$

$$v_{qr} = K_{p2}\left(K_{p1}\Delta P + K_{i1} x_1 - i_{qr}\right) + K_{i2} x_2 + s_r \omega_s L_m i_{ds} + s_r \omega_s L_{rr} i_{qr} \quad (14)$$

$$v_{dr} = K_{p2}\left(K_{p3}\Delta v + K_{i3} x_3 - i_{dr}\right) + K_{i2} x_4 - s_r \omega_s L_m i_{qs} - s_r \omega_s L_{rr} i_{dr} \quad (15)$$

where k_{p1} is the proportional power regulator gain; k_{i1} is the integrating power regulator gain; k_{p2} is the proportional gain of rotor side; k_{i2} is the integrating rotor side converter gain; k_{p3} is the proportional GSC gain; K_{i3} is the integrating GSC gain; i_{dr_ref} represents the d-axis current control component of the GSC; and i_{qr_ref} represents the q-axis current control part of the turbine side operator.

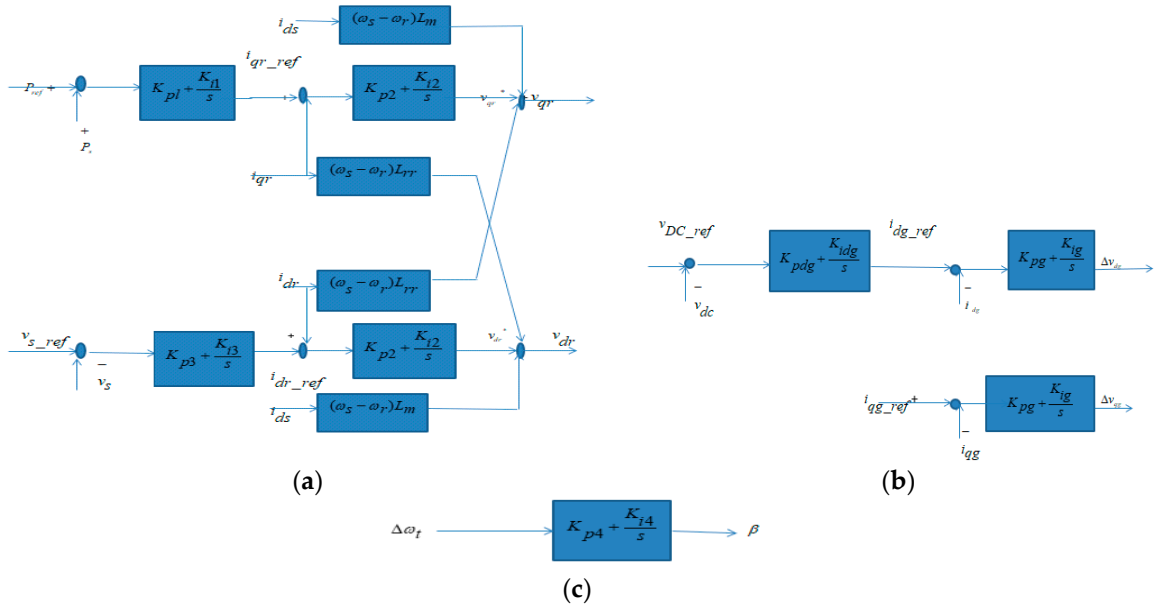

Figure 3. Control block diagram of DFIG with wind turbine (WT) (**a**) Rotor Side Converter (RSC) side, (**b**) Grid Side Converter (GCS) side, and (**c**) Pitch control [15].

Figure 3b displays the GSC block diagram. The DC voltage and the real power are regulated by converter of gird side. I_{dg} and I_{qg} are the monitor dc link voltage and reactive power, respectively, injecting x5, x6, and x7 intermediate variables, as seen in Figure 3b.

$$\frac{dx_5}{dt} = v_{DC\_ref} - v_{DC} \tag{16}$$

$$i_{dg\_ref} = -K_{pdg}\Delta v_{DC} + K_{ldg}x_5 \tag{17}$$

$$\frac{dx_6}{dt} = i_{dg\_ref} - i_{dg} = -K_{pdg\Delta v_{DC}} + K_{ldg}x_5 - i_{dg} \tag{18}$$

$$\frac{dx_7}{dt} = i_{qg\_ref} - i_{qg} \tag{19}$$

$$\Delta v_{dg} = K_{pg}\frac{dx_6}{dt} + K_{lg}X_6 = K_{pg}\left(-K_{pdg}\Delta v_{DC} + K_{ldg}x_5 - i_{dg}\right) + K_{lg}\,X_6 \tag{20}$$

$$\Delta v_{qg} = K_{pg}\frac{dx_7}{dt} + K_{ig}x_7 = K_{pg}\left(i_{qg_{ref}} - i_{qg}\right) + K_{lg}X_7 \tag{21}$$

where V_{dc_ref} is the voltage control reference of the DC link; i_{dg_ref} is the GSC current component of the q-axis; and K_{pdg} and K_{idg} are the voltage regulator proportional and integrating gains of the DC bus, respectively.

To keep the rotating speed of the wind turbine to the optimal speed, the pitch of the blade is controlled with a pitch controller. The governing equation as seen in Figure 3c is as follows:

$$\frac{d\beta}{dt} = K_{p4}\frac{T_m - T_{sh}}{2H_t} + K_{i4}\Delta\omega_t \tag{22}$$

where K_{p4} and K_{i4} are the turbine speed regulator proportional and integrating gain; T_m and T_{sh} are the mechanical torque and shaft torque; and $\Delta\omega_t$ is the deviation of turbine speed.

2.4. Dynamic Model of DFIG-Based Wind Turbine

The dynamic model of the DFIG-based wind turbine can be compactly written using above Equations (1)–(22) as

$$\dot{x} = f(x, y, z) \tag{23}$$

$$z = g(x, u) \tag{24}$$

where x = state variables of DFIG, z = output variables, and u = input variables.

From all the above given equations, the DFIG model can be written as,

$$z = \left[v_{dr}, v_{qr}, v_{dg}, v_{qg}\right]^T \quad u = [v_{ds}, v_{qs}, v_{dg}, v_{qg}]^T$$
$$x = [\omega, \beta, \theta_{tw}, s, i_{ds}, i_{qs}, E'_d, E'_q, x_1, x_2, x_3, x_4, v_{DC,} x_5, x_{6,} x_7]^T.$$

2.5. STATCOM Model

STATCOM is a parallel unit that manages the system voltage by producing reactive power for low system voltage or by absorbing reactive power at a high voltage of the system. The transformer secondary side is attached to a voltage source converter (VSC), which guarantees adequate reactive power regulations [16]. As seen in Figure 1, the performance voltages per unit (pu) q and d-axis of the suggested STATCOM may be described as follows

$$v_{qsta} = V_{dcsta} \cdot km_{sta} \cdot \cos(\theta_{bus} + \alpha_{sta}) \tag{25}$$

$$v_{dsta} = V_{dcsta} \cdot km_{sta} \cdot \sin(\theta_{bus} + \alpha_{sta}). \tag{26}$$

The equation of capacitor Cm in terms of pu DC voltage and current is given as

$$(C_m)\frac{d}{dt}(V_{dcsta}) = \omega_b\left[I_{dcsta} - \left(\frac{V_{dcsta}}{R_m}\right)\right] \tag{27}$$

$$I_{dcsta} = V_{dcsta} \cdot km_{sta} \cdot \cos(\theta_{bus} + \alpha_{sta}) + V_{dcsta} \cdot km_{sta} \cdot \sin(\theta_{bus} + \alpha_{sta}) \tag{28}$$

where

v_{qsta} and v_{dsta}	q-and d-axis voltages at the STATCOM output (pu) terminal, respectively
km_{sta}	STATCOM Modulation Index
α_{sta}	STATCOM Phase Angle
V_{dcsta}	Pu voltage of capacitor Cm

DC current I_{dcsta} is flowing through the positive side of V_{dcsta}. R_m is the per unit (pu) equal resistance (STATCOM losses are also taken in consideration); pu represents the q-and d-axis currents i_{qsta} and i_{dsta} flows, respectively, in the STATCOM ports. Panel A of Figure 4 shows the basic block presentation of suggested the STATCOM with PID controller. Similarly, panels B and C of Figure 4 show the basic control block presentation of the studied STATCOM with PID plus fuzzy and an ANFIS damping controller. V_{dcsta} represent the pu DC voltage; it is regulated through α_{sta}, whereas AC voltage v_{sta} can regulated by adjusting Km_{sta}.

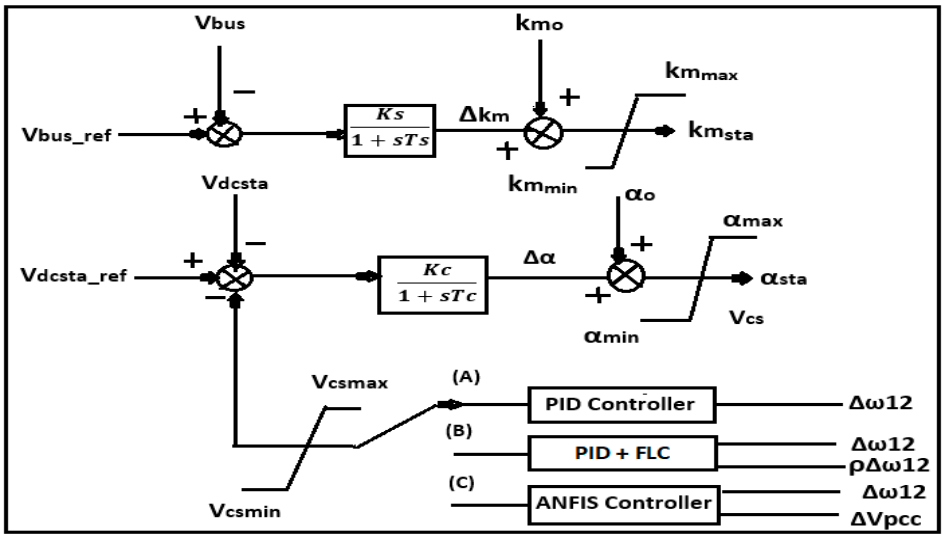

Figure 4. Static synchronous compensator (STATCOM) control unit employing the PID, hybrid PID and Fuzzy Logic Controller (FLC) and adaptive network-based fuzzy inference system (ANFIS) damping controllers.

2.6. Modeling of Three-Machine Nine-Bus System

Figure 1 shows an on-line representation of a widely popular 3-machine 9-bus network, which is frequently used for the stability analyses of the power system. This system's full parameters can be referred to ref. [17]. The simplified approaches used to analyze transient stability are commonly utilized in the activity and analysis of power systems. The following parts assume that the transient stability evaluation process has provided the following mathematics equations and resolution algorithms to illustrate the concept and strategy of simplified transient stability analysis: the constant impedance models for all loads in the network. Generator 1 employs the classical model, while Generator 2 and Generator 3 employ the double-axis model.

$$\frac{d\Delta\delta}{dt} = \omega_s \Delta\omega \tag{29}$$

$$\begin{aligned}\frac{d\Delta\omega}{dt} = \frac{1}{T_J}\{-D\,\Delta\omega - I_{q(0)}\Delta E''_q - I_{d(0)}\Delta E''_d + \Delta P_m - \left[E''_{d(0)} - \left(X''_d - X''_q\right)I_{q(0)}\right]\Delta I_d \\ -\left[E''_{q(0)} - \left(X''_d - X''_q\right)I_{d(0)}\right]\Delta I_q\}\end{aligned} \tag{30}$$

$$\frac{d\Delta E'_q}{dt} = \frac{1}{T'_{d0}}\left[-k_d\Delta E'_q + (k_d - 1)\Delta E''_q + \Delta E_{fq}\right] \tag{31}$$

$$\frac{d\Delta E''_q}{dt} = \frac{1}{T''_{do}}\left[\Delta E'_q + \Delta E''_q - (X'_d - X''_d)\Delta I_d\right] \tag{32}$$

$$\frac{d\Delta E'_d}{dt} = \frac{1}{T'_{q0}}\left[-k_q\Delta E'_d + \left(k_q - 1\right)\Delta E''_d\right] \tag{33}$$

$$\frac{d\Delta E''_d}{dt} = \frac{1}{T''_{qo}}\left[\Delta E'_d - \Delta E''_d + \left(X'_q - X''_q\right)\Delta I_q\right] \tag{34}$$

$$\Delta V_d = \Delta E''_d - R_a\Delta I_d + X''_q\Delta I_q \tag{35}$$

$$\Delta V_q = \Delta E''_q - R_a\Delta I_q - X''_d\Delta I_d \tag{36}$$

Here, $k_d = \frac{X_d - X''_d}{X'_d - X''_d}$ and $k_q = \frac{X_q - X''_q}{X'_q - X''_q}$, where ω_s is the synchronous speed; ω is the angular speed; T_j is the moment of inertia; P_m is the mechanical power output; δ is the rotor angle; R_a is the stator resistance; X_d, X_q are the synchronous reactance of the d and q-axis; the q and d-axis time constants are

T_d, T_q; V_q, V_d are the stator voltages of q and d-axis; I_q, I_d are the q and d-axis current; E_q, E_d are the q and d-axis E.M.F; E_{fq} is the generator no load synchronous voltage; (here, ', '', and o represent the transient, sub transient, and the initial values, respectively; these can be referred to Ref. [17]).

2.7. Excitation System

For example, we can derive from the linearized Equations (37)–(40) an excitation system composed of a DC-type exciter including a thyristor controller. The coordinate conversion of d, q voltage and current components in generator terminals may be defined for $V_c = \left|V + jX_cI\right|$.

Naturally, [17] the entire DC excitation method has a linear equation:

$$\frac{d\Delta E_{fq}}{dt} = -\frac{K_E + n_E c_E \left(E_{fq(0)}\right)^{n_E - 1}}{T_E}\Delta E_{fq} + \frac{1}{T_E}\Delta V_R \tag{37}$$

$$\frac{d\Delta V_R}{dt} = -\frac{1}{T_A}\Delta V_R - \frac{K_A}{T_A}\Delta V_F - \frac{K_A}{T_A}\Delta V_M + \frac{K_A}{T_A}\Delta V_S \tag{38}$$

$$\frac{d\Delta V_F}{dt} = -\frac{K_F\left(K_E + n_E c_E \left(E_{fq(0)}\right)^{n_E - 1}\right)}{T_E T_F}\Delta E_{fq} + \frac{K_F}{T_E T_F}\Delta V_R - \frac{1}{T_F}\Delta V_F \tag{39}$$

$$\frac{d\Delta V_M}{dt} = -\frac{1}{T_R}\Delta V_M + \frac{K_{cq}X_C}{T_R}\Delta I_d - \frac{K_{cd}X_C}{T_R}\Delta I_q + \frac{K_{cd}}{T_R}\Delta V_d + \frac{K_{cq}}{T_R}\Delta V_q \tag{40}$$

where $K_{cd} = \left(V_{d(0)} - X_C I_{q(0)}\right)/V_{C(0)}$, $K_{cq} = \left(V_{q(0)} + X_C I_{d(0)}\right)/V_{C(0)}$; E_{fq} = excitation voltage, V_R = excitation voltage, V_F = output of feedback unit, voltage, V_M = measured voltage. T_A and K_A are the time constant and integrated amplification device gain. The exciter control parameters are X_C, K_E, K_F, T_F, C_E, T_E, and T_R.

2.8. Prime Mover and Governing System

The linearized equation of hydraulic turbine and its governing scheme is given below [17]:

$$\frac{d\Delta\mu}{dt} = \frac{K_\delta}{K_s}\Delta\omega - \frac{1}{T_s}\Delta\xi \tag{41}$$

$$\frac{d\Delta\xi}{dt} = \frac{K_\delta\left(K_i + K_\beta\right)}{T_s}\Delta\omega + \frac{K_i}{T_i}\Delta\mu - \left(\frac{1}{T_i} + \frac{K_i + K_\beta}{T_s}\right)\Delta\xi \tag{42}$$

$$\frac{d\Delta P_m}{dt} = -\frac{2K_\delta K_{mH}}{T_s}\Delta\omega + \frac{2K_{mH}}{T_\omega}\Delta\mu + \frac{2K_{mH}}{T_s}\Delta\xi - \frac{2}{T_\omega}\Delta P_m. \tag{43}$$

μ is the position of the relay valve, ξ is a position variable exhibiting feedback from μ, K_δ is the proportional coefficient, T_s is the time constant of relay, K_i is the integral gain, K_β and T_i are the soft feedback gain and time constant, ω is the generator speed, T_ω is the relative time constant of the water hammer impact, and the hydraulic turbine's hydraulic power output is P_m. K_{mH} is given by

$$K_{mH} = \frac{P_H(MW)}{S_B(MVA)}. \tag{44}$$

2.9. Generation Module Matrix Definition

The vector that can be configured for a generating unit defined in Equations (29)–(43) is given as:

$$\Delta x_g = \left[\Delta\delta, \Delta\omega, \Delta E'_q, \Delta E''_q, \Delta E'_d, \Delta E''_d \Delta E'_{fq}, \Delta V_R, \Delta V_F, \Delta V_M, \Delta\mu, \Delta\xi, \Delta P_M\right]^T. \tag{45}$$

2.10. PID Damping Controller Design for STATCOM

A PID's damping controller concept and the STATCOM's design findings to boost stability by utilizing a coherent approach focused on the principle of modal control is addressed in this section [18]. System mathematical models established in the earlier segment are used to obtain a series of matrix-linearized model equations

$$\rho X = AX + BU + VW \tag{46}$$

$$Y = CX + DU \tag{47}$$

where X, Y are the vector of state and output, U is the external one, W is a perturbation vector and A, B, C, and D are all the stable matrices of the correct size. The X variable consists of three substate vectors as $X = [X_{SG}, X_{Wt-DFIG,} X_{STATCOM}]^T$, where respectively X_{SG}, $X_{Wt-DFIG,}$, and $X_{STATCOM}$ represent state vectors of the synchronous generator unit, the DFIG plus wind farm, and the STATCOM. Since wind rarely exceeds the normal speed of 14 m/s, the minimal working level of configuring the PID dampening regulator is correctly chosen as 12 m/s. The eigenvalues of the evaluated system without DFIG-WF and with the DFIG-WF as well as the suggested STATCOM are shown in the second and third columns of Table 1, respectively. The observed system's small signal stability analysis reveals 5 eigenvalue pairs (15 eigenvalues), consisting of 5 complex eigenvalue pairs and 10 real eigenvalues. Eigenvalues are represented as λ_1 to λ_{15}, where λ_{5-6} and λ_{7-8} are mechanical modes related to the deviation of the rotor angle between G1 and G2 and the deviation of the rotor angle between G1 and G3. λ_{11-12}, λ_{13-14} are the electrical modes, related to ΔV_R and $\Delta E'_q$, respectively. The eigenvalues' real components are negative, indicating that the device becomes small signal stable at the operating point.

Table 1. Eigenvalues of the test system [damping ratio] at 12 m/s wind speed.

Eigenvalue No.	Studied System Excluding of WF	System Including WF and STATCOM	System with Wind Farm, STATCOM, and PID Controller
λ_1	−52.79 + 0.000i	−52.654 + 0.000i	−52.986 + 0.000i
λ_2	−51.764 + 0.000i	−50.321 + 0.000i	−51.875 + 0.000i
λ_3	−30.543 + 0.000i	−30.896 + 0.000i	−30.974 + 0.000i
λ_4	−28.647 + 0.000i	−28.643 + 0.0000i	−28.647 + 0.000i
λ_{5-6}	−0.787 ± 12.8449i 0.0592	−0.538 ± 14.2469i 0.0378	−0.85 ± 14i 0.060
λ_{7-8}	−0.531 ± 8.9071i 0.0795	−0.486 ± 8.0504i 0.061	−0.90 ± 8i 0.1117
λ_9	−4.4512 ± 0.4563i	−4.8762 ± 0.4657i	−4.7651 ± 0.4342i
λ_{10}	−0.1919 + 0.00i	−0.1754 + 0.00i	−0.2112 + 0.00i
λ_{11-12}	−1.135 ± 3.3182i	−1.2311 ± 3.658i	−2.9077 ± 4.212i
λ_{13-14}	−0.4501 ± 0.618i	−0.4501 ± 0.718i	−0.5765 ± 0.438i
λ_{15}	−7.5477	−7.7609	−7.6654

The proper values given in Table 1 refer to the studied system modes. After the addition of STATCOMs with a PID damping function, the test device modes are almost set on the complex plane. The modes and the deviation of the rotor angle among G1 and G2 as well as the deviation of the rotor angle among G1 and G3 are changed, so damping controls may boost these modes. The STATCOM control block diagram, along with the model PID damping mechanism, can be seen in panel A of Figure 4.

A PID damping controller on the first command detects the G1 and G2 ($\Delta\omega 12$) rotor speed variance to produce a signal to increase the damping factors of the studied mechanism described in

Table 1 for two modes (λ_{5-6} and λ_{7-8}). The s domain transfer function for the STATCOM shown in Figure 4 including PID is given as

$$H(s) = \frac{U(s)}{Y(s)} = \frac{V_{cs}}{\Delta\omega_{12}} = \frac{sT_w}{1+sT_w}\left(K_p + \frac{K_I}{s} + sK_D\right) \quad (48)$$

where T_w = time constant, and K_p, K_I, and K_D reflect the gain of the PID controller. Using the Laplace transformation to achieve the characteristic polynomial of the PID controller,

$$U(s) = H(s)\Delta\omega_{12}(s) = H(s)Y(s) = H(s)CX(s). \quad (49)$$

We get from (47) and (48):

$$sX(s) = \{A + B[H(s)]\}X(s). \quad (50)$$

The characteristic polynomial of the system with PID controller indicated as

$$\det\{sI - [A + B[H(s)]\} = 0. \quad (51)$$

The four damping parameters of the PID are obtained by replacing two pairs of given modes (λ_{5-6} and λ_{7-8}) in Equation (51).

Predefined eigenvalues $\lambda_{5-6} = -0.85 \pm i14$ and $\lambda_{7-8} = -0.90 \pm i8$.

The above parameters are specified as

$$K_P = -48.34,\ K_I = -185,\ K_D = -33.36,\ T_W = 0.42.$$

In Table 1, the fourth column, along with the planned PID damping controller, specifies the eigenvalues of the tested bus system comprising the DFIG-WF and the planned STATCOM. It can be clearly observed that on the complex plane, both λ_{5-6} and λ_{7-8} have been located precisely at the appropriate positions. In comparison, the damping ratios rise from 0.0378 to 0.0601 and 0.0610 to 0.1117. Many criteria for choosing the assigned eigenvalues could be explicitly assigned eigenvalues as alluded to Ref. [18,19]. Based on the four constants of the STATCOM model, the PID dampening regulator described earlier, and the results of above table, it can be concluded that the implementation findings are suitable for the system being investigated.

2.11. PID Plus FLC Damping Controller Desgin for STATCOM

Throughout this segment, the theory technique Fuzzy Logic Control (FLC) is used to construct the hybrid damping system PID and FLC shown in panel B of Figure 4. The following measures are used to construct the FLC system: (1) fuzzification, (2) decision-making logic, (3) defuzzification, and (4) knowledge base (KB). Figure 5 shows the schematic presentation of this combined PID plus FLC controller; here, the FLC is fed by rotor speed variance w_{12} and its differential $p(w_{12})$ to produce three gains (K'_p, K'_i, and K'_D) to add to the gains of the configured PID controller in the preceding paragraph to control the phase angle of the STATCOM. Using the following rules, such incremental gains from the FLC are compared to the PID controller gains [20,21].

$$K_{ph} = K_p + K'_p,\ K_{Ih} = K_I + K'_I,\ K_{Dh} = K_D + K'_D \quad (52)$$

In this case, FLC is based on the Sugeno-type fuzzy inference method, since it fits well for dimensional, optimizing, and responsive approaches. It includes seven linguistic variables for each input element. Variables include NB (Negative Big), NM (Negative Medium), NS (Negative Small), ZR (Zero), PS (Positive Small), PM (Positive Medium), and PB (Positive Big). In addition, it also has seven linguistic output variables, namely IB (Increase Big), IM (Increase Medium), IS (Increase Small),

KV (Keep Value), DS (Decrease Small), DM (Decrease Medium), and DB (Decrease Big). Table 2 lists the regulation laws for the two input signals and the output signal.

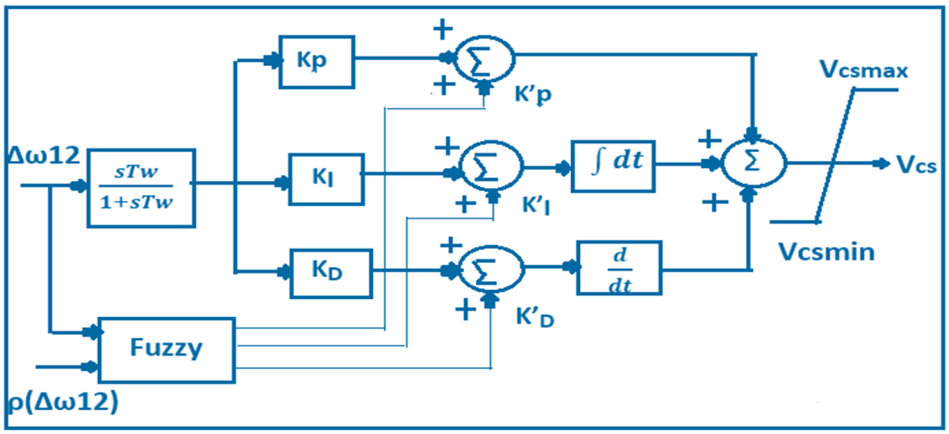

Figure 5. Diagram of the combined PID and FLC scheme [19].

Table 2. Regulation laws of the observed FLC.

Δω12 / P(Δω12)	NB	NM	NS	ZR	PS	PM	PB
PB	KV	IS	IM	IB	IB	IB	IB
PM	DS	KV	IS	IM	IB	IB	IB
PS	DM	DS	KV	IS	IM	IB	IB
ZR	DB	DM	DS	KV	IS	IM	IB
NS	DB	DB	DM	DS	KV	IS	IM
NM	DB	DB	DB	DM	DS	KV	IS
NB	DB	DB	DB	DB	DM	DS	KV

2.12. ANFIS Damping System Configuration for STATCOM

The controlling diagram for STATCOM along with the configured ANFIS damping system was displayed in panel C of Figure 4. In order to produce a control signal Vcs for modulation of the STATCOM's phase angle (αSTA), the ANFIS control unit is fed by rotor-speed variance of the SG between 1 and 2 (Δω12) and the voltage variance of the PCC (ΔVPCC). The following simple measures are employed to develop the ANFIS controller for the STATCOM: (1) data creation, (2) features of rules extraction and membership, (3) training as well as testing, and (4) outcomes [13]. The Sugeno configuration is used for the proposed ANFIS, wherein the guidelines for the framework are as follows

$$(fi = p_i x_1 + q_i x_2 + r_i) \text{ if } (x_1 = A_i) \text{ and } (x_2 = B_i). \quad (53)$$

In the above equation, $(x_1 = \Delta\omega)$ and $(x_2 = \Delta V_{PCC})$ are used as an input; the fuzzy set is specified by A_i and B_i; f_i is the value inside the fuzzy field defined by the fuzzy law. The parameters set up throughout the training phase are p_i, q_i and r_i, and i is the quantity of membership functions for each input parameter. With each input variable, seven linguistic variables are included in this work as described in the previous section: NB, NM, NS, ZR, PS, PM, and PB. The output variable also includes seven linguistic variables, which are the same as the fuzzy output variables: IB, IM, IS, KV, DS, DM, and DB. Two ANFIS control variables ((Δω) and (ΔV_{PCC})) are also included. Table 2 lists the control rules that are applicable to the input signals and the output element. The ANFIS model structure is shown in Figure 6. The components of the ANFIS method are similar to those of the standard fuzzy method, except that a layer of secret neurons is calculated at each point. More information is provided in five layers. The neuron in the first layer (inputs) corresponds to a linguistic variable, whereas the

output is equivalent to the linguistic variable's membership function. In the second layer (function of input membership), each node multiplies the incoming signals and sends out the component reflecting the firing intensity of a law. The third layer node (law) measures the ratio of the fire power of the ith rule firing to the sum of the firing intensity of all the laws. Throughout the fourth layer (output membership function), the performance is the sum of the ith rule and rules previously discovered relative to the firing power. The total output is determined as the addition of incoming signals by the final layer (production). ANFIS is tested using the MATLAB toolbox. Table 3 represents the ANFIS Editor parameters as given below.

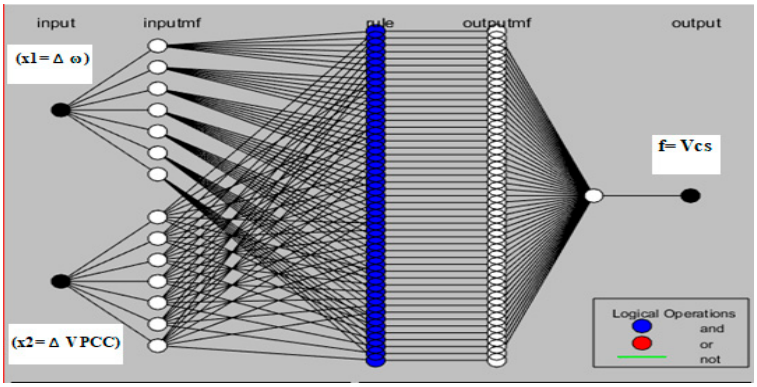

Figure 6. ANFIS model structure.

Table 3. ANFIS parameters.

Membership function type	Gauss
Number of epochs	30
Learning algorithm	Hybrid (mixed least squares and back-propagation)
Total nodes	131
Linear parameters (no.)	49
Nonlinear parameters (no.)	42
Total number of parameters	91
Training data pairs	5288
Fuzzy rules	49

For ANFIS training, the information is drawn from the examined system's results with the planned PID including an FLC dampening controller with a 3-phase short circuit disturbance at bus 5. Figure 7a maps the performance of the configured PID including the FLC controller as performance training statistics for ANFIS (blue patterns) and training statistics after developed ANFIS (red asterisks). From this figure, it can be found that the output signal exhibits improved damping efficiency following training of the design ANFIS (red asterisks). Illustration Figure 7b demonstrates the regulation surface between the two inputs (input 1 = ΔV_{PCC} and input 2 = $\Delta\omega$) and the related output (V_{cs}), respectively.

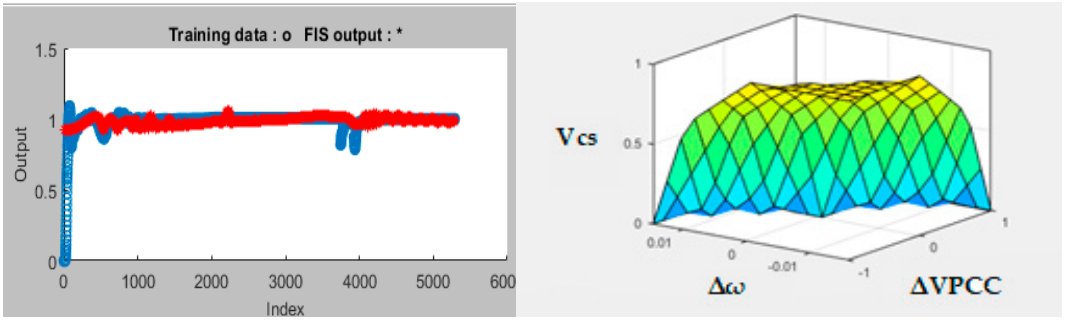

(**a**) (**b**)

Figure 7. ANFIS training data outcome and control surface. (**a**) Training data outcome. (**b**) Suggested ANFIS control surface.

3. Results

This segment employs the nonlinear model of the system configured in the third segment to test the damping dynamics provided by the suggested STATCOM together with the modeled PID controller, the combined PID including FLC, and the ANFIS damping controller to increase the stability of the system being tested under a three-phase short-circuit failure on bus 5 of Figure 1. The short-circuit fault with three phases is immediately introduced to bus 5 at 30 s, and it is resolved at 30.1 s. While this form of failure occurs barely in practical energy systems, testing whether the devices can survive these extreme device impacts, it is the most serious and the most dangerous failure. When the systems being studied are reliable while this extreme fault is unexpectedly introduced and certain defensive relays clear it, the systems being studied have the potential to stay reliable as they are exposed to certain faults such as single line-to-ground faults, line-to-line faults, etc. The DFIG-based WF is presumed to operate at a wind speed of 12 m/s, whereas the three-machine device runs under controlled conditions as alluded to in ref [22]. In this section, the figure demonstrates the analyzed system's comparative transient responses.

Figures 8 and 9 represent the transient response of the test system under a 3-phase short-circuit fault without a controller (green line), with a PID controller (yellow line), with a hybrid PID with FLC (red line), and with the proposed STATCOM with ANFIS controller (black line).

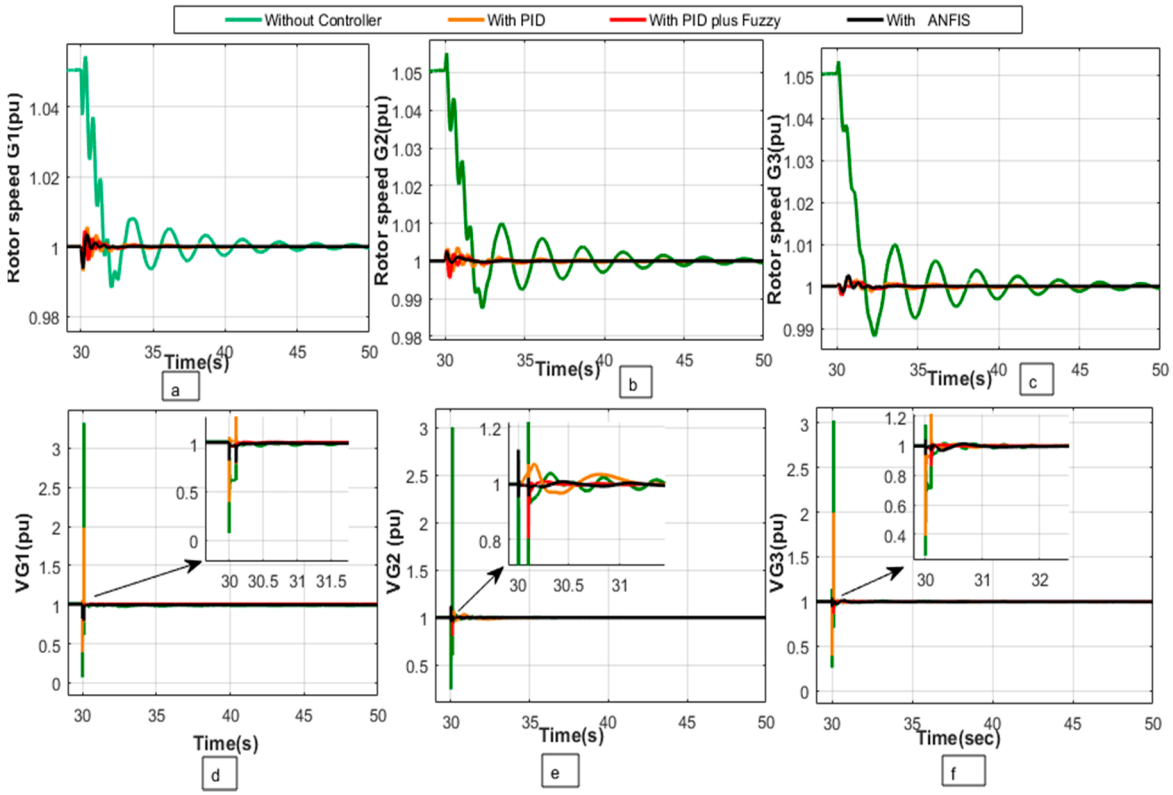

Figure 8. Studied system transient response under 3-phase short circuit fault: (**a**) SG1 Rotor speed; (**b**) SG2 Rotor speed; (**c**) SG3 Rotor speed; (**d**) SG1 terminal voltage; (**e**) SG2 terminal voltage; (**f**) SG3 terminal voltage.

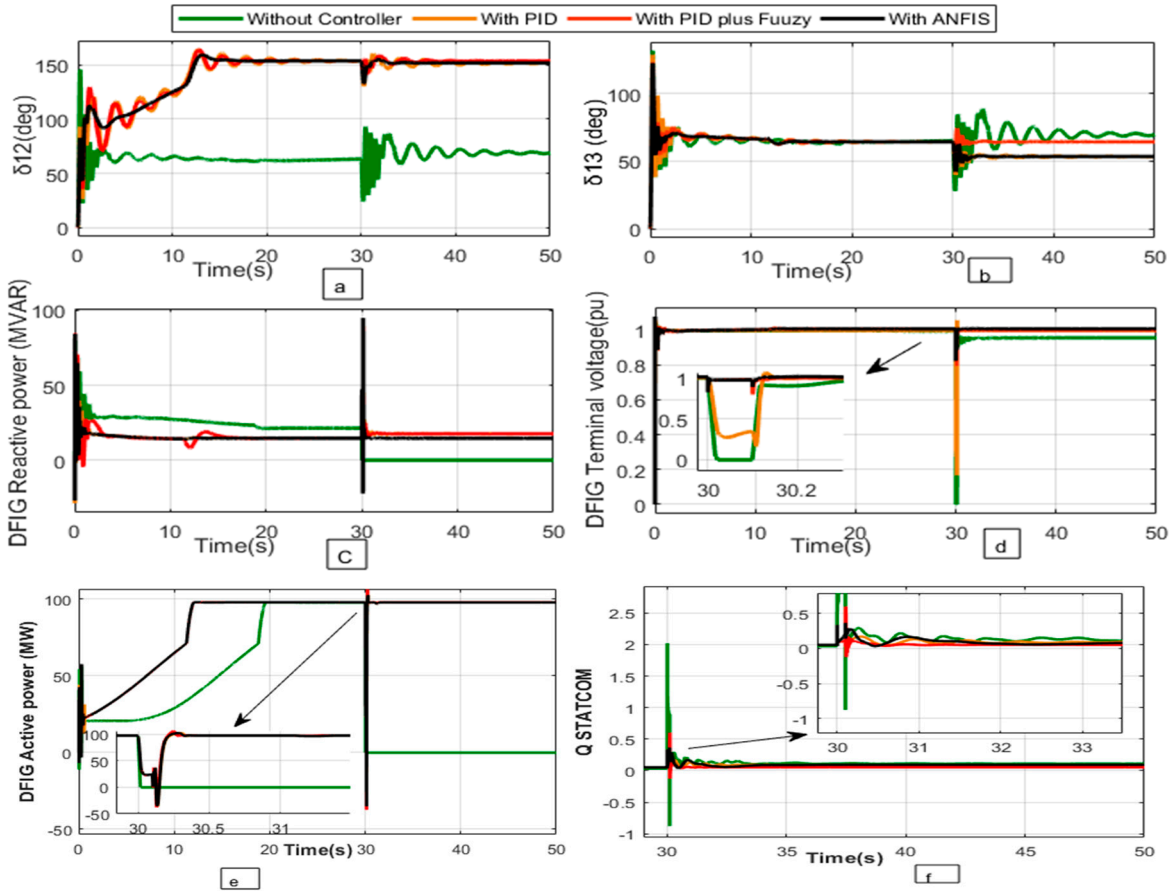

Figure 9. Studied system parameters during fault: (**a**) rotor angle deviation between SG1 and SG2; (**b**) rotor angle deviation between SG1 and SG3; (**c**) DFIG reactive power; (**d**) DFIG terminal voltage (output voltage); (**e**) DFIG active power; (**f**) STATCOM reactive power.

4. Discussion

The comparative discussions of the previous section simulation results are given in this section. The speeds of synchronous generators are shown in Figure 8a–c. Without any controller, synchronous generators take more time to achieve steady-state speed due to insufficient damping. In the presence of a damping controller, STATCOM with PID plus fuzzy oscillation damped, and alternators G1, G2, and G3 settle in 4, 5, and 6 s, respectively. Furthermore, in the presence of a damping controller, the STATCOM with ANFIS transient response of the rotor speed was greatly improved compared to PID and PID plus fuzzy-controlled STACOM.

The terminal voltages of synchronous generators are shown in Figure 8d–f. In the presence of STATCOM with an ANFIS controller, the transient response of the terminal voltages of G1, G2, and G3 improved. The DFIG-based WF responses are displayed in Figure 9c–f. Initially, the wind speed is adjusted to 8 m/s; therefore, the wind speed raises abruptly to 12 m/s at t = 5 s. At t = 5 s, the active power produced begins to increase smoothly (along with the turbine speed) to achieve the rated power of 100.5 MW in 19 s without any controller, as shown in Figure 9e. However, in the presence of Fuzzy plus PID and an ANFIS controller, it reaches its rated value before 19 s. Figure 9a,b shows the result of rotor angle deviation between G1 and G2 and G1 and G3, respectively, for without a controller, with a STATCOM PID controller, STATCOM with a hybrid PID plus Fuzzy controller, and STATCOM plus an ANFIS controller. The dynamic time response of the rotor angle deviation is improved by the ANFIS controller. As the system is exposed to LLL failure, DFIG trips because its output voltage reduces below 0 pu due to wind turbine protection. In the presence of STATCOM with a PID controller, STATCOM with PID plus FLC and STATCOM with an ANFIS controller DFIG retain their output

voltages of 0.45 pu, 0.80 pu, and 0.91, respectively, as shown in Figure 9d. The DFIG reactive power supply reduces to 14.65 MVAR in an ANFIS-controlled system, as displayed in Figure 9c. Figure 9f shows the reactive power generated by STATCOM. It shows better dynamic response in the case of an ANFIS controller.

Transient findings are displayed in Figures 8 and 9. The essential efficacy of ANFIS in damping the studied method is compelling, as ANFIS is a very powerful approach to constructing a dynamic and nonlinear relationship between the input and output dataset. ANFIS may also incorporate both numerical and linguistic information into a fuzzy law through the use of fuzzy methods. The fuzzy membership functions can be optimally balanced by using the error back-propagation algorithm in this analysis. ANFIS also has its nonlinear capability, fast learning, and adaptive capabilities.

The suggested ANFIS system is learned from the studied system's transient responses with the proposed STATCOM in conjunction with the developed Fuzzy plus PID controller; the device responses along with the proposed STATCOM in conjunction with the ANFIS provide the better damping output. Alternatively, we can say that STATCOM and ANFIS achieve steady-state values, and the system's transient responses are the quickest. Other transient responses have very similar characteristics, which may include the strongest damping characteristics for the device tested with a combination of the proposed STATCOM and ANFIS method.

This reveals that the suggested STATCOM with an ANFIS controller will provide the studied device with sufficient reactive power and improve the damping characteristics to easily dampen the intrinsic oscillations of the tested system as opposed to the tested system without a controller, with a PID, and a PID plus fuzzy controller.

5. Conclusions

This article addressed the DFIG-based Wind Farm's stability improvement linked to a 3-machine 9-bus network utilizing a STATCOM coupled with a built PID damping system, PID plus FLC system, and an ANFIS device. The STATCOM is suggested and is attached to the system's PCC to provide appropriate reactive control. For the STACOM, a PID damping controller was developed using a unified approach focused on modal control theory to delegate the studied Synchronous Generator (SG)'s mechanical mode and exciter mode. Time-domain simulations of the device undergoing a three-phase short-circuit failure at the PCC were conducted to assess the efficacy of the suggested STATCOM in conjunction with the developed PID damping controller, PID Plus FLC, and the suggested STATCOM in conjunction with the developed ANFIS damping controller to suppress the studied system's intrinsic SG oscillations and boost the system stability. From the simulation results, it can be inferred that the suggested STATCOM in conjunction with the developed ANFIS damping controller provides better damping efficiency under an extreme disruption situation of the studied DFIG-based wind farm-linked power system. The nonlinear device ANFIS can address the multiple operating points of the system. In fact, ANFIS is also a tool of adaptation and robustness, as it incorporates the benefits of ANN and FLC.

Author Contributions: V.K. proposed the test system and did the MATLAB simulation related work. A.S.P. supervised the work and provided help in the original draft preparation. S.K.S. also gave supervision and guided the mathematical modeling of the system. All authors have read and agreed to the published version of the manuscript.

Funding: This research was funded by Technical Education Quality Improvement Program (TEQIP-III), KNIT Sultanpur.

Conflicts of Interest: The authors declare no conflict of interest.

Abbreviations

The following abbreviations are used in this manuscript:

WF	Wind Farm
STATCOM	Static Synchronous Compensator
DFIG	Double-Fed Induction Generator
FLC	Fuzzy Logic Controller
ANFIS	Adaptive network-based fuzzy inference system
BESS	Battery Energy Storage System
PCC	Point of Common Coupling
LVRT	Low Voltage Ride Through
SVC	Static VAR Compensator
SMES	Superconducting Magnetic Energy Storage
PSS	Power System Stabilizer
SSSC	Static Synchronous Series Compensator
CWF	Combined wind farm
MOGA	Multiobjective Genetic Algorithm based
WOA	Whale optimization algorithm
SGs	Synchronous Generators
RSC	Rotor Side Converter
GSC	Grid Side Converter

References

1. Wang, L.; Wang, K.H. Dynamic stability analysis of a DFIG-based offshore wind farm connected to a power grid through an HVDC link. *IEEE Trans. Power Syst.* **2010**, *26*, 1501–1510. [CrossRef]
2. Muljadi, E.; Nguyen, T.B.; Pai, M.A. Impact of wind power plants on voltage and transient stability of power systems. In Proceedings of the Conference on IEEE Energy 2030, Atlanta, GA, USA, 17–18 November 2008.
3. Pokharel, B.; Gao, W. Mitigation of disturbances in DFIG-based wind farm connected to weak distribution system using STATCOM. In Proceedings of the IEEE Conference on North American Power Symposium (NAPS), Arlington, TX, USA, 26–28 September 2010.
4. Mak, L.O.; Ni, Y.X.; Shen, C.M. STATCOM with fuzzy controllers for interconnected power systems. *Elect. Power Syst. Res.* **2000**, *55*, 87–95. [CrossRef]
5. Reznik, L.; Ghanayem, O.; Bourmistrov, A. PID plus fuzzy controller structures as a design base for industrial applications. *Eng. Appl. Artif. Intell.* **2000**, *13*, 419–430. [CrossRef]
6. Molinas, M.; Suul, J.A.; Undeland, T. Low voltage ride through of wind farms with cage generators: STATCOM versus SVC. *IEEE Trans. Power Electron.* **2008**, *23*, 1104–1117. [CrossRef]
7. Hemeida, M.G.; Rezk, H.; Hamada, M.M. A comprehensive comparison of STATCOM versus SVC-based fuzzy controller for stability improvement of wind farm connected to multi-machine power system. *Springer Electr. Eng.* **2018**, *100*, 935–951. [CrossRef]
8. Muyeen, S.M.; Hasanien, H.M.; Al-Durra, A. Transient stability enhancement of wind farms connected to a multi-machine power system by using an adaptive ANN-controlled SMES. *Energy Convers. Manag.* **2014**, *70*, 412–420. [CrossRef]
9. Ni, Z.; Tang, Y.; Sui, X.; He, H.; Wen, J. An adaptive neuro-control approach for multi-machine power systems. *Electr. Power Energy Syst.* **2016**, *75*, 108–116. [CrossRef]
10. Taj, T.A.; Hasanien, H.M.; Alolah, A.I.; Muyeen, S.M. Transient stability enhancement of a grid connected wind farm using an adaptive neuro fuzzy controlled-flywheel energy storage system. *IET Renew. Power Gener.* **2015**, *9*, 792–800. [CrossRef]
11. Ibrahim, Y.; Kamel, S.; Rashad, A.; Nasrat, L.; Jurado, F. Performance Enhancement of Wind Farms Using Tuned SSSC Based on Artificial Neural Network. *Int. J. Interact. Multimed. Artif. Intell.* **2019**, *5*, 1–7. [CrossRef]
12. Rashad, A.; Kamel, S.; Jurado, F.; Abdel-Nasser, M.; Mahmoud, K. ANN-Based STATCOM Tuning for Performance Enhancement of Combined Wind Farms. *Electr. Power Compon. Syst.* **2019**, *47*, 10–26. [CrossRef]

13. Jang, J.S. ANFIS: Adaptive-network-based fuzzy inference system. *IEEE Trans. Syst. Man Cybern.* **1993**, *23*, 665–685. [CrossRef]
14. Muyeen, S.M.; Ali, M.H.; Takahashi, R.; Murata, T.; Tamura, J.; Tomaki, Y.; Sakahara, A.; Sasano, E. Transient stability analysis of wind generator system with the consideration of multi-mass shaft model. In Proceedings of the International conference on Power Electronics and Drives Systems, Kuala Lumpur, Malaysia, 28 November–1 December 2005.
15. Wu, F.; Zhang, X.P.; Godfrey, K.; Ju, P. Small signal stability analysis and optimal control of a wind turbine with doubly fed induction generator. *Gener. Transm. Distrib. IET* **2007**, *1*, 751–760. [CrossRef]
16. Wang, L.; Hsiung, C.T. Dynamic stability improvement of an integrated grid-connected offshore wind farm and marine-current farm using a STATCOM. *IEEE Trans. Power Syst.* **2011**, *26*, 690–698. [CrossRef]
17. Wang, X.F.; Song, Y.; Irving, M. *Modern Power Systems Analysis*; Springer Science & Business Media: New York, NY, USA, 2010.
18. Ma, J.; Dong, Z.Y.; Zhang, P. Eigenvalue sensitivity analysis for dynamic power system. In Proceedings of the International Conference on Power System Technology, (POWERCON 2006), Chongqing, China, 22–26 October 2006.
19. Wang, L.; Truong, D. Stability Enhancement of DFIG-Based Offshore Wind Farm Fed to a Multi-Machine System Using a STATCOM. *IEEE Trans. Power Syst.* **2013**, *28*, 2882–2889. [CrossRef]
20. Lee, C. Fuzzy logic in control system: Fuzzy logic controller, Part I and II. *IEEE Trans. Syst. Man Cybern.* **1990**, *20*, 404–435. [CrossRef]
21. Mansour, I.; Abdeslam, D.O.; Wira, P.; Merckle, J. Fuzzy logic control of a SVC to improve the transient stability of ac power systems. In Proceedings of the 2009 35th Annual Conference of IEEE Industrial Electronics, Porto, Portugal, 3–5 November 2009.
22. Anderson, P.M.; Fouad, A.A. *Power System Control and Stability*; Iowa State Univ. Press: Ames, IA, USA, 1977.